Integrative Biology

Accepted Manuscript

ROYAL SOCIETY OF CHEMISTRY

www.rsc.org/ibiology

INSIGHT, INNOVATION, INTEGRATION

B-precursor acute lymphoblastic leukemia (BPL) is the most common form of childhood and adolescent cancer. Despite major improvements in survival outcome of newly diagnosed BPL patients treated on contemporary chemotherapy protocols, achieving long-term leukemia-free survival in the majority of patients who fail their frontline chemotherapy regimen and relapse remains an unmet medical need in BPL therapy. Here we first report a unique biotargeted nanoscale liposomal nanoparticle (LNP) formulation of the spleen tyrosine kinase (SYK) P-site inhibitor C61 decorated with a CD19-specific monoclonal antibody. This unique pharmaceutical composition targeting the SYK-dependent anti-apoptotic blast cell survival machinery shows promise for overcoming the clinical radiochemotherapy resistance of BPL cells.

CD19-antigen specific nanoscale liposomal formulation of a SYK P-site inhibitor causes apoptotic destruction of human B-precursor leukemia cells

Dorothea E. Myers,[1] Seang Yiv,[1] Sanjive Qazi,[1] Hong Ma[1], Ingrid Cely,[1] Anoush Shahidzadeh,[1] Martha Arellano-Garcia[1], Erin Finestone[1], Paul Gaynon,[1,2] Amanda Termuhlen,[2,3] Jianjun Cheng,[4] Fatih Uckun[1,2,5]

[1]Developmental Therapeutics Program, Children's Center for Cancer and Blood Diseases, Children's Hospital Los Angeles (CHLA), Los Angeles, CA 90027; [2]Division of Hematology-Oncology, Department of Pediatrics; [3]Jonathan Jaques Cancer Center, Miller Children's Hospital, Long Beach, CA 90806; [4]Department of Materials Science and Engineering, University of Illinois at Urbana–Champaign (UIUC), Urbana, Illinois 61801; [5]Developmental Therapeutics Program, Norris Comprehensive Cancer Center, University of Southern California Keck School of Medicine (USC KSOM), Los Angeles, CA 90027

***Corresponding author**: Fatih M. Uckun, M.D., Ph.D., Children's Center for Cancer and Blood Diseases, Children's Hospital Los Angeles, MS#160, Los Angeles, California 90027-0367. E-mail: fmuckun@chla.usc.edu; Phone: (323)-361-4328

Abstract

We report the anti-leukemic potency of a unique biotargeted nanoscale liposomal nanoparticle (LNP) formulation of the spleen tyrosine kinase (SYK) P-site inhibitor C61. C61-loaded LNP were decorated with a murine CD19-specific monoclonal antibody directed against radiation-resistant CD19-receptor positive aggressive B-precursor acute lymphoblastic leukemia (ALL) cells. The biotargeted C61-LNP were more potent than untargeted C61-LNP and consistently caused apoptosis in B-precursor ALL cells. The CD19-directed C61-LNP also destroyed B-precursor ALL xenograft cells and their leukemia-initiating *in vivo* clonogenic fraction. This unique nanostructural

therapeutic modality targeting the SYK-dependent anti-apoptotic blast cell survival machinery shows promise for overcoming the clinical radiochemotherapy resistance of B-precursor ALL cells.

Insight, Innovation, Integration

B-precursor acute lymphoblastic leukemia (ALL) is the most common form of childhood and adolescent cancer. Despite major improvements in survival outcome of newly diagnosed B-precursor ALL patients treated on contemporary chemotherapy protocols, achieving long-term leukemia-free survival in the majority of patients who fail their frontline chemotherapy regimen and relapse remains an unmet medical need in B-precursor ALL therapy. Here we first report a unique biotargeted nanoscale liposomal nanoparticle (LNP) formulation of the spleen tyrosine kinase (SYK) P-site inhibitor C61 decorated with a CD19-specific monoclonal antibody (MoAb). This unique pharmaceutical composition targeting the SYK-dependent anti-apoptotic blast cell survival machinery shows promise for overcoming the clinical radiochemotherapy resistance of B-precursor ALL cells.

Introduction

B-precursor ALL is the most common form of cancer in children and adolescents [1]. Despite major improvements in survival outcome of newly diagnosed B-precursor ALL patients on contemporary chemotherapy protocols [1-3], achieving long-term leukemia-free survival in the majority of patients who fail frontline chemotherapy and relapse remains an unmet medical need [4-11]. SYK is a cytoplasmic protein tyrosine kinase with multiple important regulatory functions in B-lineage lymphoid cells [12,13]. Constitutive activation and anti-apoptotic function of SYK is documented for several B-lineage lymphoid malignancies, including B-precursor ALL [14-16]. SYK functions as a master regulator of apoptosis controlling the activation of the PI3-K/AKT, NFκB, and STAT3 pathways - three major anti-apoptotic signaling pathways in B-precursor ALL cells [14]. We recently identified the pentapeptide mimic 1,4-bis (9-*O*-dihydroquinidinyl) phthalazine/hydroquinidine 1,4-phathalazinediyl diether (“compound 61”) (C61) as a highly selective and potent inhibitor targeting

the substrate binding P-site of SYK [15, 16] Unlike available inhibitors of SYK that target the ATP binding site, C61 targets the tyrosine kinase substrate-binding site of SYK. C61 thereby provides a unique opportunity to selectively target the SYK-dependent anti-apoptotic survival machinery in leukemic B-cell precursors [15]. Notably, *in vitro* disruption of the SYK-STAT3 network with C61 augmented oxidative stress-induced apoptosis of primary leukemic cells from relapsed B-precursor ALL patients [15].

By "decorating" nanoscale liposomal nanoparticles carrying C61 as the payload with PEGylated anti-CD19 monoclonal antibody (Ab) molecules, we developed a multifunctional LNP formulation of C61. This C61-LNP-Ab provides a unique nanoscale CD19-specific pharmaceutical composition for therapeutic application against CD19-receptor positive B-precursor ALL. The purpose of the present study was to characterize this formulation and evaluate its anti-leukemic potency against primary leukemia cells from B-precursor ALL patients. We demonstrate that C61-LNP-Ab is more potent than untargeted C61-LNP and consistently causes apoptosis in radiation-resistant primary human B-precursor ALL cells. C61-LNP-Ab was also capable of destroying B-precursor ALL xenograft cells and their leukemia-initiating *in vivo* clonogenic fraction. This unique pharmaceutical composition targeting the SYK-dependent anti-apoptotic blast cell survival machinery may be useful in overcoming the clinical radiochemotherapy resistance of B-precursor ALL cells.

Materials and Methods

1,4-Bis(9-*O*-dihydroquinidinyl) phthalazine/hydroquinidine 1,4-phathalazinediyl diether (C61) and its nanoscale liposomal formulation. C61 is a potent and selective chemical inhibitor of SYK [15,16]. Dipalmitoyl phosphatidylcholine (DPPC), cholesterol (CHOL), and 1,2-dioleoyl-3-trimethylammonium-propane chloride salt (DOTAP) were obtained from Avanti Polar Lipids (Alabaster, AL). LBA and sucrose were obtained from Sigma (St Louis, MO). DSPE-PEG3400-NHS (the N-succinimidyl derivative of 1,2-distearoyl-*sn*-glycero-3-phosphoethanolamine-*N*-[methoxy(polyethylene glycol)-3400] ("DSPE-PEG3400-NHS") was obtained from Nanocs, Inc. (New York, NY). PD-10 desalting columns packed with Sephadex G-25 medium were obtained from

GE Healthcare (Piscataway, NJ). The liposomal C61 nanoparticle formulation, C61-LNP, was prepared via the standard thin film evaporation method [17] in a round bottom flask using a fixed 26.2:13.8:3.0 ratio of DPPC: CHOL: DOTAP. The chloroform used in the LNP formulation was removed using a rotary evaporator at 40^{o}C. Entrapment of C61 was obtained using the pH gradient procedure with 0.3 M lactobionic acid (LBA) as a low pH buffer inside the LNPs. The LBA solution was added to the LNP film and the film was hydrated slowly with gentle hand mixing or by rocking the flask at ambient temperature for about 1 hour or until all the film was dispersed to yield a milky suspension. In order to obtain a nano-sized homogeneous LNP formulation, the suspension was placed in the chamber of an extruder, and extrusion was performed at 60^{o}C, twice through a 0.2 μm, then 5 times through a 0.1 μm polycarbonate filter. To establish a pH gradient, the external phase of the extruded preparation was passed through a PD-10 desalting column packed with Sephadex G-25 medium, which had been pre-equilibrated with 10% sucrose in water. After this external phase replacement step, C61 was added and the preparation was stirred at room temperature for 60 min to allow C61 to cross into the acidic interior of the LNPs. After the completion of the drug addition, the pH was adjusted upward to about 6.5 by the addition of sodium hydroxide solution. In the final step, the C61-LNP formulation was filter sterilized through 0.22 μm filters and stored in a 4^{o}C refrigerator. We decorated C61-LNP with an in-house prepared anti-CD19 mouse monoclonal antibody (MoAb) (IgG2a) secreted by the hybridoma cell line ARESX1 developed using previously published standard methods [18]. To determine the unique cDNA sequence of the complementarity determining regions (CDR) of this MoAb, mRNA was extracted from around 10^{7} ARESX1 hybridoma cells using Qiagen Oligotex mRNA Mini kit (Cat. No70022). The first-strand cDNA was generated with oligo (dT) primers using Superscript III reverse transcriptase (Invitrogen, San Diego, CA). The cDNA fragments encoding the heavy chain and the light chain variable regions were then obtained by PCR using the high fidelity Phusion kit (E0553s, New England Biolabs) with the Heavy Primers Mix (Cat NO 27-1586-01, GE Healthcare) and the Light Primers Mix (Cat No 27-1583-01, GE Healthcare), respectively. The VH (~390-bp) and VL (~320-bp) PCR products were subsequently ligated to the pCR4Blunt-TOPO vector (Cat. No K2835-20, Invitrogen) for DNA sequencing using universal

forward (GTAAAACGACGGCCAG) and reverse (CAGGAAACAGCTATGAC) primers (Cat. No N520-02 and N530-02). One unique VH fragment and one VL fragment were identified. The corresponding CDRs were determined using the Immunogenetics (IMGT) database [http://www.imgt.org] (**Figure 1**). The MoAb isolated from mouse ascites fluid produced by the ARESX1 hybridoma line was centrifuged at high speed to remove debris, lipids, etc. prior to purification on a Protein A column using the Affi-Gel Protein A MAPS II kit from Bio-Rad Laboratories. The clarified ascites was diluted with an equal volume of the binding buffer contained in the kit and applied to a protein A column equilibrated in the same binding buffer at a pH of 8.8 – 9.2. The column was washed with binding buffer until the A280 reading dropped below 0.05. The MoAb was then eluted at a pH of 2.8 – 3.0, with the elution buffer contained in the kit. Fractions containing the majority of the protein were combined and immediately neutralized. Pre-packed PD-10 columns (GE Healthcare) were subsequently used to equilibrate the MoAb into PBS, pH 7.4 prior to testing or further use in preparation of C61-LNP-Ab. Purified anti-CD19 Moab at a final concentration of 6 mg/mL (0.04 μmols/mL) was reacted with a 20:1 molar ratio of DSPE-PEG3400-NHS: MoAb. The DSPE-PEG-NHS was dissolved in DMSO, and 65 μL (0.8 μmols) were added to the MoAb in PBS. The mixture was rotated in a controlled-temperature chamber for 4h at 35^{o}C. Unreacted DSPE-PEG-NHS and small molecular weight reaction products were removed by passing the mixture through a pre-packed PD-10 size exclusion column (GE Healthcare Life Sciences, Piscataway, NJ) equilibrated in PBS (10 mM sodium phosphate, 138 mM NaCl, 2.7 mM KCl), pH 6.5. The fractions containing the majority of the MoAb were combined, concentrated, and mixed with C61-loaded C61-LNP according to a standard post-insertion procedure. This mixture was rotated in the controlled-temperature chamber at 45^{o}C for 6 h and then applied to a 1.6 x 40 cm Sephacryl S-300 HR size-exclusion column to separate the antibody-decorated C61-LNP (C61-LNP-Ab) from uninserted, modified anti-CD19 MoAb. The column was equilibrated in PBS, pH 7.4, at a flow rate of 0.5 mL/min. The optical density of the fractions eluting approximately 40 min after loading was followed at 600 nm. These fractions contained C61-LNP-Ab and were very cloudy and white. When the readings at 600 nm approached baseline, the OD was read at 280 nm to monitor

the elution of the uninserted MoAb. The peak of antibody typically eluted between 70 and 80 min after loading. Size measurement by the dynamic light scattering (DLS) technique, Zeta potential measurements, analytical high performance liquid chromatography (HPLC) and transmission electron microscopy (TEM) were used for physicochemical characterization of the C61-LNP-Ab. We used a dot blot assay to confirm the presence of the MoAb molecules in the C61-LNP-Ab liposomal nanoparticles. The decorating antibody both in unmodified form (concentration range: 0.3-1000 μg/mL) as well as DSPE-PEG modified form (concentration range: 0.2-600 μg/mL) used for post-insertion and non-PEGylated C61-LNP were included as controls. The dot blots were performed on PVDF membranes using both a polyclonal rabbit anti-PEG antibody as well as a polyclonal goat-anti-mouse antibody. The immunoreactive dots were visualized by chemiluminescence, as described in Materials and Methods. In brief, two microliters of each sample were dot blotted onto a PVDF membrane (Millipore) and allowed to dry for 1 hour. Membranes were blocked with 5% milk in Tris buffered saline with Tween 20 (TBST) buffer (20 mM Tris pH 7.5, 150 mM NaCl, 0.1% Tween 20) for 1 h and then incubated in primary antibody for 1 hour. For anti-PEG blot analysis, the polyclonal rabbit anti-Polyethylene glycol (PEG-B-47) was used as the primary antibody at a 1:5000 dilution (Abcam, Cat# 51257). Following incubation with this primary antibody, the membranes were washed 3 times with 1X TBST buffer. The membranes were blotted for 1 h with the horseradish peroxidase (HRP)-conjugated goat-anti-rabbit IgG (Santa Cruz Biotechnology Cat#sc-2004) at a 1:2000 dilution as the secondary antibody. For anti-mouse IgG blot analysis, we used the goat anti-mouse IgG-HRP from Santa Cruz Biotechnology (Cat#sc-2005) at a 1:2000 dilution. The dots were visualized by chemiluminescence detection reagent (GE Healthcare). The immunoreactivity of the C61-LNP-Ab with the CD19-receptor positive B-precursor ALL cell line ALL-1 was examined by standard indirect immunofluorescence and flow cytometry using FITC- or PE-labeled goat anti-mouse (GAM) antibodies to detect its cell-bound murine CD19 MoAb moiety, as previously described [19,20]. The T-lineage ALL cell lines MOLT-3 and CEM served as CD19 receptor-negative control cell lines to demonstrate that C61-LNP-Ab binds to CD19 receptor-positive but not to CD19 receptor-negative leukemia cells. In stability experiments, C61-LNP-Ab was incubated for indicated

time periods ranging from 15 min to 24 h with serum obtained from primary bone marrow aspirate samples of pediatric B-precursor ALL patients at a 1:1 volume: volume ratio. Subsequently, dot plot analysis using the goat anti-mouse IgG-HRP as well as flow cytometric immunoreactivity analysis using the FITC-labeled GAM antibody were performed. Control samples were incubated with serum-free RPMI tissue culture medium instead of human serum.

Physicochemical Characterization of Nanoparticles. Size measurement by the dynamic light scattering (DLS) technique was performed on a DynaPro Titan Instrument (Wyatt Technology Corp., Santa Barbara, CA) at the USC Nano BioPhysics Laboratory. A sample volume of 20 µl was loaded into a quartz cell for the DLS analysis. The particle size was obtained by averaging the data obtained for at least 10 measurements with 10 sec per acquisition. For the measurement of C61 concentrations, C61-LNP and C61-LNP-Ab samples were analyzed on an Agilent 1100 HPLC system equipped with a Hypersil ODS reverse phase analytical column (Hewlett Packard Hypersil 5 µm ODS, 125 x 4.6 mm) and a diode array detector with detection and reference wavelengths set at 230 nm and 420 nm, respectively. Acetonitrile: water (20:80 v/v) containing 0.1% trifluoroacetic acid and 0.1% triethylamine was used as the mobile phase. The Zeta potential measurements were carried out on a Brookhaven Instrument ZetaPlus (Holtsville, NY).

Transmission Electron Microscopy (TEM). The morphology of the C61-LNP-Ab was examined using TEM, as previously described [17]. In brief, samples of liposomal nanoparticle formulations were diluted 1:1 with 2% uranyl acetate and placed on Formvar-coated copper grids (300 Mesh) for 5 min. The samples were then gently blotted against clean filter paper and air dried for 10 min. Grids were examined on a JEOL JEM-2100 LaB6 (Peabody, MA) transmission electron microscope and photographed with the Orius SC1000B Gatan (Pleasanton, CA) digital camera.

Cells. Leukemia cells from 4 patients with B-precursor ALL (Primary leukemia cells from 3 patients and xenograft cells derived from one patient) as well as 5 ALL cell lines (CD19 receptor-positive cell lines = DAUDI: Burkitt's leukemia/B-cell ALL, NALM-6: B-precursor ALL and ALL-1: BCR-ABL$^+$ B-precursor ALL; CD19 receptor-negative cell lines: MOLT-3 and CEM: T-lineage ALL), were used in the described experiments. We also used a previously described B-precursor ALL xenograft model

[17]. The secondary use of leukemic cells for subsequent molecular studies did not meet the definition of human subject research per 45 CFR 46.102 (d and f) since it does not include identifiable private information. The project was approved by the IRB (CCI) at the Children's Hospital Los Angeles (CHLA) (Human Subject Assurance Number: FWA0001914) and Memorialcare Health System Institutional Review Board at Miller Children's Hospital, Long Beach, CA.

Irradiation of cells. Cells were irradiated with 200 cGy gamma (γ)-rays using a self-shielded Cs-137 irradiator (Mark I Irradiator-6BA, JL Sheperd & Associates, San Fernando, CA), as previously reported [17]. All personnel using the irradiator completed the "Radiation Safety Training for Operators of Cs-137 Irradiators" and completed formal operational training in the safe and proper operation of the irradiator in compliance with the radiation safety procedures of the Children's Hospital Los Angeles and as directed by the CHLA Radiation Safety Officer.

Apoptosis Assays. We used both primary B-precursor ALL cells as well as ALL cell lines in the described experiments. 24h or 48h after continuous exposure to C61-LNP-Ab or the control reagents C61-LNP and Ab alone, cells were analyzed for apoptosis using the standard quantitative flow cytometric apoptosis assay using the Annexin V-FITC Apoptosis Detection Kit from Sigma, as previously reported [17]. The labeled cells were analyzed on a LSR II flow cytometer. Viable cells don't bind to PI or Annexin V FITC and therefore reside in the left lower quadrant. When the cells become apoptotic, they start binding to Annexin V FITC and shift to the right. Early apoptotic cells reside in the right lower quadrant. As apoptosis advances, the nuclear membrane breaks down and the cells show nuclear staining with PI. Therefore they also show a shift along the Y-axis. Therefore, cells with advanced apoptosis reside in the right upper quadrant. When cells lose most of their cytoplasm, the Annexin V FITC staining is lost and the dead cells are located in the left upper quadrant. The anti-leukemic potency of various treatments was documented by the significantly lower percentages of Annexin V-FITC$^-$PI$^-$ live cells located in the left lower quadrant of the corresponding two-color fluorescence dot plots as well as a substantially higher percentage of Annexin V-FITC$^+$PI$^+$ advanced stage apoptotic cells located in the right upper quadrant. The

percentages for Annexin V-FITC$^-$PI$^-$ viable cells and Annexin V-FITC$^+$PI$^+$ advanced apoptotic cells for each sample are indicated in the respective quadrants of the two-color fluorescence dot plots. Pairwise Two-sample Student's T-tests for differences between means were performed to assess the significance of the differences in percent viability of leukemic cells post-treatment between C61-LNP-Ab treatments vs. controls/non-leukemic mice as well as treatments with unmodified C61-LNP. P-values of less than 0.05 were deemed significant and not corrected for multiple comparisons as the false discovery rate was less than 5% for the planned limited number of comparisons that were performed.

SCID Mouse Xenograft Model of Human B-Precursor ALL. We used a NOD/SCID mouse model of human B-precursor ALL. NOD/SCID mice (NOD.CB17-*Prkdc*^{scid}/J; 4-6 weeks of age at the time of purchase, female) were obtained from the Jackson Laboratory (Sacramento, CA). The research was conducted according to Institutional Animal Care and Use Committee (IACUC) Protocol #280-09 entitled “Evaluation of Tyrosine Kinase Inhibitors Against Childhood Leukemia in Immunodeficient Mice”, that was approved by the IACUC of CHLA on 11-24-2009 and its 3-year rewrite application 280-12 that was approved on 7-10-2012. All animal care procedures conformed to the Guide for the Care and Use of Laboratory Animals (National Research Council, National Academy Press, Washington DC 1996, USA). ALL xenograft cells (Cell density: 2x10^6 cells/mL) isolated from spleens of leukemic NOD/SCID mice challenged with primary leukemic cells from a pediatric B-precursor ALL patient were treated with D5W (CON), C61-LNP-Ab (C61 concentration: 30 μg/mL), 200 cGy γ-rays, C61-LNP-Ab (C61 payload: 30 μg/mL) + 200 cGy γ-rays or left untreated for 24 h at 37^{o}C. Following treatment, xenograft cells were reinjected into NOD/SCID mice ((Pretreatment cell number of inoculum samples: 250,000 cells/mouse) in order to evaluate the *in vitro* potency of the treatments against the leukemic stem cell fraction capable of engrafting and causing overt leukemia in NOD/SCID mice. Mice were monitored daily and electively euthanized by CO_2 asphyxia on day 151 after 2 control mice developed fatal leukemia at 146 days and 151 days, respectively. At the time of their death or elective sacrifice, mice were necropsied to confirm leukemia-associated marked splenomegaly. Spleens of mice were removed, measured, and cell suspensions were

prepared for determination of nucleated cell counts. Multiple organs were preserved in 10% neutral phosphate buffered formalin, and processed for histologic sectioning. For histopathologic studies, formalin fixed tissues were dehydrated and embedded in paraffin by routine methods. Glass slides with affixed 4-5 micron tissue sections were prepared and stained with Hemotoxylin and Eosin (H&E). Brain, liver, kidney, lymph nodes, and bone marrow were examined for their leukemic involvement. Two-sample Student's T-tests (pooled variances) were performed to assess the significance of the differences in spleen size and log-transformed spleen nucleated cell counts of NOD/SCID mice challenged with xenograft cells treated with C61-LNP-Ab vs. controls (no treatment control and radiation control). P-values of less than 0.05 were deemed significant and not corrected for multiple comparisons as the false discovery rate was less than 5% for the planned limited number of comparisons that were performed. For the analysis of the *in vitro* potency of various treatments against leukemic stem cells in xenograft specimens, two-tailed T-tests with correction for unequal variance (Microsoft, Excel) were performed comparing the mean spleen size and cellularity for the various treatments. Controls for baseline values of spleen size and nucleated spleen cell count were non-leukemic NOD/SCID mice that had not been inoculated with any leukemia cells.

Results

Characterization of C61-LNP. The C61-LNP formulation was prepared by using the thin film evaporation method with the use of DPPC (26.2 mg/ml), CHOL (13.8 mg/mL), DOTAP (3.0 mg/mL) and the entrapment of C61 within the interior space of LNP was achieved using a pH gradient procedure that employs (LBA, 300 mM). The generated unmodified C61-LNP had a mean diameter of 135.8±1.0 nm (N=10), a positive surface charge with a Zeta potential of 38.8±0.6 mV in solution consistent with the use of positively charged DOTAP and contained 9.4±0.1 mg/mL C61. After decoration of the C61-LNP with DSPE-PEG3400-NHS modified anti-CD19 MoAb, the biotargeted C61-LNP-Ab were separated from uninserted anti-CD19 MoAb using a Sephacryl S-300 HR size-exclusion column (**Figure 2A**). SDS-PAGE, run under nonreducing conditions and followed by Coomassie Blue staining of the eluting antibody-decorated C61-LNP ("C61-LNP-Ab") fraction F1

confirmed the presence of both antibody and lipid (from A), (**Figure 2B**). Dot blot analysis of C61-LNP-Ab using anti-PEG as well as anti-moue IgG antibodies confirmed the presence of DSPE-PEG modified MoAb in the liposomal nanoparticles (**Figure 2C**). Particle size (radius) measurement of the C61-LNP-Ab using dynamic light scattering indicated a mean diameter of 154.2±1.9 nm (**Figure 2D**). After decoration with negatively charged anti-CD19 MoAb molecules, the Zeta potential was reduced to 4.1±0.2 mV (**Figure 2E**). The TEM images of the C61-LNP-Ab are depicted in **Figure 2F**. C61-LNP-Ab appeared stable at 37^{o}C in the presence of human serum obtained from primary bone marrow aspirate samples of pediatric B-precursor ALL patients at a 1:1 volume: volume ratio and incubation times ranging from 15 min to 24h (**Figure 3**). The selective immunoreactivity of the C61-LNP-Ab with CD19-receptor positive B-precursor ALL cells was confirmed by indirect immunofluorescence and flow cytometry using the ALL-1 cell line (**Figure 4**). C61-LNP-Ab did not bind to CD19-receptor negative T-lineage ALL cell lines MOLT-3 or CEM as it did to ALL-1 cells. The small percentage of MOLT3 and CEM cells (<15%) showing above background fluorescence likely reflect the ability of liposomes to interact with cellular membranes or non-specific binding of the Fc-domain of the Ab to surface Fc-receptors. The poor binding of C61-LNP-Ab to the CD19-receptor negative T-lineage ALL cell lines was not a false negative result caused by a technical problem related to the secondary antibody GAM-FITC, because the latter antibody exhibited strong binding to the murine hybridoma cell line ARESX1 expressing the antibody moiety of C61-LNP-Ab on its surface. C61-LNP-Ab caused apoptosis in the CD19^{+} ALL-1 B-precursor ALL cell line. The anti-leukemic potency of C61-LNP-Ab against ALL-1 cells was evidenced by a substantially higher percentage of Annexin V-FITC^{+}PI^{+} apoptotic cells located in the right upper quadrant of the corresponding two-color fluorescence density plots of the cells (from 4% in CON to 80% after C61-LNP-Ab treatment) within the encircled P1 lymphoid window concomitant with a marked shrinkage and altered SSC as well as decreasing numbers of the remaining cells in the P1 lymphoid window in the corresponding FSC/SSC light scatter plot (from 73% in CON to 18% after C61-LNP-Ab treatment) (**Figure 5**). C61-LNP-Ab did not kill CD19^{-} MOLT-3 T-lineage ALL cells, consistent with its CD19-restricted cytotoxic action (**Figure 5**). Unlike C61-LNP-Ab, C61-LNP did not cause

apoptosis in ALL-1 cells (**Figure 5**) demonstrating that the decoration of C61-LNP with the anti-CD19 MoAb augments its cytotoxic activity against $CD19^+$ leukemia cells. The resistance of MOLT-3 cells to C61-LNP-Ab was not caused by an inherent resistance to its payload C61, as C61 caused apoptosis in MOLT-3 cells at both 10 μg/mL and 30 μg/mL concentrations (**Figure 5**).

***In vitro* anti-leukemic activity of C61-LNP against radiation-resistant human B-precursor ALL cells.** We next used quantitative flow cytometric apoptosis assays to evaluate the ability of the unmodified vs. antibody-decorated C61-LNP to induce apoptosis in B-precursor ALL cells. Both formulations were highly effective in causing apoptosis of the Burkitt's leukemia/B-cell ALL cell line DAUDI (**Figure 6**). By comparison, C61-LNP-Ab was more effective than C61-LNP against the adult B-precursor ALL cell lines ALL-1 (Figure 5) and pediatric B-precursor ALL cell line NALM-6 (Figure 6) as well as primary leukemia cells from 3 pediatric patients with B-precursor ALL (PT1 and PT2 depicted in Figure 6; all 3 patients along with NALM-6 cell line depicted in **Figure 7**). The cumulative data for pediatric B-precursor ALL cells (i.e., NALM-6 cell line and primary leukemia cells from 3 patients) are shown in **Figure 7**. Statistical analysis of the apoptosis data confirmed that C61-LNP-Ab was significantly more potent than unmodified C61-LNP (**Figure 7**).

We next sought to evaluate the ability of the C61-LNP-Ab formulation to kill very aggressive B-precursor ALL xenograft cells as well as their leukemia-initiating *in vivo* clonogenic fraction. C61-LNP-Ab caused apoptosis reducing the viability of the xenograft cells from 72.1% to 1.3%. By comparison, radiation with 2 Gy γ-rays reduced the viability to 45.6% (**Figure 8 A**). Xenograft cells isolated from spleens of leukemic NOD/SCID mice were treated with C61-LNP-Ab (C61 concentration: 30 μg/mL), 2 Gy γ-rays, C61-LNP-Ab + 2 Gy γ-rays or left untreated for 24 h at 37°C. Following treatment, xenograft cells were reinjected into NOD/SCID mice ((Pretreatment cell number of inoculum samples: 250,000 cells/mouse). Control mice challenged with untreated xenograft cells invariably developed overt leukemia between 146 days and 151 days. Necropsy revealed massive splenomegaly at the time of death with a nucleated cell count of $>100x10^6$ cells/spleen in 5 of 5 mice

(100 %) (**Figure 8B-D**). Likewise, 2 of 3 mice challenged with irradiated xenograft cells developed fatal leukemia with massive splenomegaly. By comparison, none of the 3 mice injected with C61-LNP-Ab treated xenograft cells and none of the 5 mice injected with xenograft cells treated with C61-LNP-Ab + radiation developed leukemic splenomegaly (**Figure 8B&C**) (i.e., 7 of 8 controls vs. 0 of 8 test mice, Fisher's Exact, 2-tailed, P=0.0014). The average spleen size 3.7 ± 0.1 cm ("massive enlargement") for the control mice (N=5), 2.8 ± 0.7 cm ("enlarged") for the radiation alone group (N=3), 1.5 ± 0.03 cm ("not enlarged") for the C61-LNP-Ab alone group (N=3; P-value <0.0001 compared to control, P = 0.0044 compared to Radiation alone, P=0.6 compared to non-leukemic controls) and 1.6 ± 0.1 cm ("not enlarged") for the C61-LNP-Ab + radiation group (N=5; P-value <0.0001 compared to control, P = 0.0029 compared to radiation alone, P=0.4 compared to non-leukemic controls) (**Figure 8C**). The average spleen nucleated cell count (in millions) as a measure of the leukemic burden was 598 ± 195 ("very high"; $\log_{10}$ = 2.68 ± 0.15) for the control group (N=5), 17 ± 6 ("normal", $\log_{10}$ = 1.17 ± 0.17; P-value = 0.0008 compared to control, P=0.2 compared to non-leukemic controls) for C61-LNP-Ab alone, and 8 ± 2 ("normal"; $\log_{10}$ = 0.86 ± 0.10; P-value < 0.0001 compared to control; P-value = 0.0046 compared to radiation alone, P=0.5 compared to non-leukemic controls) for the combined C61-LNP-Ab + radiation group (**Figure 8D**). These findings demonstrate that C61-LNP-Ab alone or in combination with low dose radiation damages the *in vivo* clonogenic fraction in xenograft cell populations derived from patients with aggressive B-precursor ALL and abrogates their ability to engraft and cause overt leukemia in NOD/SCID mice.

Discussion

Liposomal nanoparticle therapeutics containing cytotoxic agents may provide the foundation for potentially more effective and less toxic anti-cancer treatment strategies due to their improved pharmacokinetics, reduced systemic toxicity, and increased intra-tumoral/intra-cellular delivery [21-23]. Nanoparticles can be functionalized with a tumor targeting moiety, such as a ligand or an antibody directed against a surface receptor on cancer cells in order to achieve optimal tumor targeting and site-specific drug delivery to further reduce their toxicity and improve their efficacy [24-

28]. When linked with tumor targeting moieties nanoparticles can reach cancer cells carrying the target receptors with high affinity and precision [24-28]. The targeting ligands enable nanoparticles to bind to cell surface receptors and enter cells by receptor-mediated endocytosis [28].

CD19 is a B-lineage specific 95 kDa surface receptor, which is expressed on leukemia cells from 85% of patients with ALL (100% of patients with B-precursor ALL), but is absent on the parenchymal cells of life-maintaining non-hematopoietic organs, circulating blood myeloid and erythroid cells, T-cells as well as bone marrow stem cells [20, 29, 30]. CD19 is found on the surface of each leukemic B-precursor ALL blast cell at a high density (>50,000 molecules/cell), shows a high affinity for native and engineered recombinant anti-CD19 MoAb/antibody fragments (K_a>10^8 M^{-1}), undergoes antibody induced internalization upon binding of anti-CD19 MoAb, and it is not shed from the surface [20, 29-31]. CD19 has also been found on *in vivo* clonogenic B-precursor ALL cells with leukemia initiating and propagating properties in xenograft models using immunocompromised mice [32-34]. The favorable leukemic cell vs. normal tissue expression profile of CD19 and its abundant expression on relapse B-precursor ALL clones make it an attractive molecular target for biotherapy in relapsed B-precursor ALL using anti-CD19 immunoconjugates [35, 36], bispecific T-cell engaging antibodies [37] as well as targeted T-cell therapy using autologous T cells expressing a CD19-specific chimeric antigen receptor (CAR) [38]. Therefore, anti-CD19 MoAb also show potential as targeting molecules to selectively deliver nanoparticles loaded with apoptosis-inducing cytotoxic agents to $CD19^+$ B-precursor ALL cells. Recently, Zhang et al. reported the successful preparation of sterically stabilized liposomes modified with an anti-CD19 MoAb of IgM subtype and demonstrated that these CD19-specific nanoparticles bind to and are internalized by the $CD19^+$ B-lineage ALL cell line NALM-6 [39]. Cheng et al. prepared anti-CD19 scFv coated liposomes loaded with doxorubicin and demonstrated that these CD19-directed LNP selectively bind to and are internalized by $CD19^+$ B-lineage lymphoma cells and are more potent than Caelyx, the commercial formulation of non-targeted liposomal doxorubicin [25]. In the current study, we prepared C61-LNP-Ab as multifunctional liposomal nanoparticles targeted to the CD19 receptor on B-precursor ALL cells. The

payload of C61-LNP-Ab is a highly selective and potent inhibitor of SYK, an anti-apoptotic protein tyrosine kinase that has been shown to regulate multiple biochemical signaling pathways vital to the survival of B-precursor ALL cells [14-16]. Our experiments demonstrated that this biotargeted version of C61-LNP is more potent than untargeted C61-LNP and consistently causes apoptosis in B-precursor ALL cell lines as well as primary leukemia cells from B-precursor ALL patients. *In vitro* treatment with the CD19-directed C61-LNP also destroyed B-precursor ALL xenograft cells and their leukemia-initiating *in vivo* clonogenic fraction. This unique pharmaceutical composition targeting the SYK-dependent anti-apoptotic blast cell survival machinery shows promise for overcoming the clinical radiochemotherapy resistance of B-precursor ALL cells. The focus of our next study will be the evaluation of the in vivo toxicity, pharmacokinetics, and anti-leukemic efficacy of C61-LNP-Ab as a next step toward preclinical evaluation of its clinical potential. We postulate that the nanotechnology-enabled delivery of C61 to leukemia cells will require lower systemic exposure levels for therapeutic efficacy and thereby significantly broaden the therapeutic window of this promising new anti-leukemia agent. We recently reported that a non-targeted nanoscale liposomal formulation of C61 had a very favorable safety profile in mice and exhibited potent anti-leukemic activity at nontoxic dose levels [17]. Therefore, we are optimistic that C61-LNP-Ab will also exhibit very favorable pharmacodynamics features in preclinical animal models.

MoAb and their fragments can cause potentially life-threatening immunotoxicity, including cytokine storms, anaphylaxis and anaphylactoid reactions, as well as autoimmunity. C61-LNP-Ab should be considered a partially MoAb-based therapeutic that could also cause similar side effects in clinical settings. Therefore, it will be important to carefully examine its potential immunotoxicological effects in a pharmacologically relevant animal species (e.g. a primate model) prior to a first-in-human clinical trial. The risk of immunosuppression due to a C61-LNP-Ab mediated B-cell depletion with an increased susceptibility to infections is a real possibility as with any biotherapeutic agent targeting antigens expressed on B-cells. Due to the presence of CD19 on normal human B-cells and B-cell precursors, lymphotoxicity with reduced B-cell numbers and possible hypogammaglobulinemia with

an increased risk of infections are anticipated side effects of C61-LNP-Ab in future clinical settings.

Acknowledgments

The project described was supported in part by DHHS grants P30CA014089, U01-CA-151837 and R01CA-154471 (F.M.U) from the National Cancer Institute and the NIH Director's New Innovator Award 1DP2OD007246 (J.C). The content is solely the responsibility of the authors and does not necessarily represent the official views of the National Cancer Institute or the National Institutes of Health. This work was also supported in part by Nautica Triathalon and its producer Michael Epstein (F.M.U) and Saban Research Institute Merit Awards (F.M.U). We further thank Mrs. Parvin Izadi of the CHLA Bone Marrow Laboratory, Mrs. Tsen-Yin Lin of the CHLA FACS Core, Dr. Nickolas Chelyapov of the USC NanoBiophysics Core Facility as well as Ernesto Barron and Anthony Rodriguez of the USC Norris Comprehensive Cancer Center Cell and Tissue Imaging Core for their assistance. The authors have no financial interest in the development of C61 or its liposomal formulation.

Authorship

Contribution: All authors have made significant and substantive contributions to the study. All authors reviewed and revised the paper. S.Y. designed, prepared, and partially characterized the physicochemical characteristics of C61-loaded LNP formulation and D.E.M. decorated the C61-LNP with anti-CD19 MoAb. H.M. determined the CDR sequences. S.Q performed the statistical analyses. I.C, A.S., M.A., E.F. performed multiple experiments and collected data. E.F. prepared the final figures. J.C performed the Zeta potential measurements on the C61-LNP-Ab. P.G. and A.T. evaluated pediatric leukemia patients for study eligibility and obtained bone marrow/blood specimens. F.M.U. was the NIH-funded Principal Investigator who designed, directed and supervised this study and wrote the final manuscript.

Conflict-of-interest disclosure: The authors declare no competing financial interests.

Correspondence to: Fatih M. Uckun, M.D., Ph.D., Children's Hospital Los Angeles, MS#160, Los Angeles, California 90027-0367. E-mail: uckun@usc.edu; Phone: (323)-361-4328

References

1. M.E. Trigg, P. Gaynon, F.M. Uckun. Acute lymphoblastic leukemia in children. In: *Cancer Medicine Fourth Edition* Eds: James F. Holland, Emile Fry III, Robert C. Bast, Jr., Donald W. Kufe, Donald L. Morton, Ralph R. Weichselbaum. 1996; Chapter 164, pp. 2945-2960.

2. M. Stanulla, M. Schrappe. Treatment of childhood acute lymphoblastic leukemia. *Semin Hematol,* 2009, **46**, 52-63

3. M.E. Trigg, H. Sather, G.H. Reaman, D.G. Tubergen, P.G. Steinherz, P.S. Gaynon, et al. Ten-year survival of children with acute lymphoblastic leukemia: a report from the Children's Oncology Group. *Leukemia and Lymphoma,* 2008, **49**,1142-54

4. P.S. Gaynon, R.E. Harris, A.J. Altman, B.C. Bostrom, J.C. Brenneman, R. Hawks, et al. Bone marrow transplantation versus prolonged intensive chemotherapy for children with acute lymphoblastic leukemia and an initial bone marrow relapse within 12 months of the completion of primary therapy: Children's Oncology Group Study CCG-1941. *J Clin Oncol* , 2006, **24**, 3150-3156

5. C. Uderzo, V. Conter, G. Dini, F. Locatelli, R. Miniero, P. Tamaro. Treatment of childhood acute lymphoblastic leukemia after the first relapse: curative strategies. *Haematologica,* 2001, **86**, 1-7

6. J.M. Chessells, P. Veys, H. Kempski, P. Hanley, A. Leiper, D. Webb, et al. Long-term follow-up of relapsed childhood acute lymphoblastic leukaemia. *Br J Haematol* , 2003, **123**, 396-405

7. G.K. Rivera, Y. Zhou, M.L. Hancock, A. Gajjar, J. Rubnitz, R.C. Ribeiro, et al. Bone marrow recurrence after initial intensive treatment for childhood acute lymphoblastic leukemia. *Cancer,* 2005, **103**, 368-76

8. H.G. Einsiedel, A. von Stackelberg, R. Hartmann, R. Fengler, M. Schrappe, G. Janka-Schaub, et al. Long-term outcome in children with relapsed ALL by risk-stratified salvage therapy: results of trial acute lymphoblastic leukemia-relapse study of the Berlin-Frankfurt-Münster Group 87. *J Clin Oncol,* 2005, **23**, 7942-50

9. F. Locatelli, M. Schrappe, M.E. Bernardo, S. Rutella, How I treat relapsed childhood acute lymphoblastic leukemia. *Blood*, 2012, **120**, 2807-16

10. S. Malempati, P.S. Gaynon, H. Sather, M.K. La, L.C. Stork. Outcome after relapse among children with standard-risk acute lymphoblastic leukemia: Children's Oncology Group study CCG-1952. *J Clin Oncol,* 2007, **25**, 5800-7

11. L.C. Bailey, B.J. Lange, S.R. Rheinhold, N.J. Bunin. Bone marrow relapse in paediatric acute lymphoblastic leukemia. *Lancet Oncol,* 2008, **9**, 873-83

12. A.M. Cheng B. Rowley, W. Pao, A. Hayday, J.B. Bolen, T. Pawson. Syk tyrosine kinase required for mouse viability and B-cell development. *Nature*, 1995, **378**, 303-306.

13. A. Mocsai, J. Ruland, V.L. Tybulewicz. The SYK tyrosine kinase: a crucial player in diverse biological functions. *Nat Rev Immunol*, 2010, **10**, 387-402.

14. F.M. Uckun, S. Qazi. Spleen tyrosine kinase as a molecular target for treatment of leukemias and lymphomas. *Expert Rev Anticancer Ther*, 2010, **10**, 1407-18.

15. F.M. Uckun, S. Qazi, H. Ma, L. Tuel-Ahlgren, Z. Ozer. STAT3 is a substrate of SYK tyrosine kinase in B-lineage leukemia/lymphoma cells exposed to oxidative stress. *Proc. Natl. Acad. Sci. USA*, 2010, **107**, 2902-7.

16. F.M. Uckun, R.O. Ek, S.T. Jan, C.L. Chen, S. Qazi. Targeting SYK Kinase-Dependent Anti-Apoptotic Resistance Pathway in B-lineage Acute Lymphoblastic Leukemia (ALL) Cells with a Potent SYK Inhibitory Pentapeptide Mimic. *British Journal of Haematology,* 2010, **149**, 508-17.

17. F.M. Uckun, S. Qazi, I. Cely, K. Sahin, A. Shahidzadeh, I. Ozercan, et al. Nanoscale liposomal formulation of a SYK P-site inhibitor against B-precursor leukemia. *Blood*, 2013, **121**, 4348-54. doi: 10.1182/blood-2012-11-470633. Epub 2013 Apr 8.

18. F.M. Uckun. Monoclonal antibody specific for human B-cells US Patent Publication US4831117A. Publication date: May 16, 1989.

19. F.M. Uckun, W.E. Evans, C.J. Forsyth, K.G. Waddick, L.T. Ahlgren, L.M. Chelstrom, et al. Biotherapy of B-cell precursor leukemia by targeting genistein to CD19-associated tyrosine kinases. *Science* (Washington DC), 1995, ***267,*** 886-891.

20. F.M. Uckun, W. Jaszcz, J.L. Ambrus, A.S. Fauci, K. Gajl-Peczalska, C.W. Song, et al. Detailed studies on expression and function of CD19 surface determinant by using B43 monoclonal antibody and the clinical potential of anti- CD19 immunotoxins. *Blood*, 1988, ***71,*** 13-29.

21. M.E. Davis, Z. Chen, D.M. Shin. Nanoparticle therapeutics: an emerging treatment modality for cancer. *Nature Review Drug Discovery*, 2008, 7, 771-82

22. K. Cho, X. Wang, S. Nie, Z.G. Chen, D.M. Shin. Therapeutic nanoparticles for drug delivery in cancer. *Clin Cancer Res*, 2008, **14**, 1310-6.

23. R. Sinha, G.J. Kim, S. Nie, D.M. Shin. Nanotechnology in cancer therapeutics: bioconjugated nanoparticles for drug delivery. *Mol Cancer Ther,* 2006, **5**, 1909-17.

24. W.W.K. Cheng, D. Das, Suresh M, Allen TM. Expression and purification of two anti-CD19 single chain Fv fragments for targeting of liposomes to CD19-expressing cells. *Biochimica Biophysica Acta, 2007,* **1768**, 21-29

25. Cheng WWK, T.M. Allen. Targeted delivery of anti-CD19 liposomal doxorubicin in B-cell lymphoma: A comparison of whole monoclonal antibody, Fab' fragments and single chain Fv. *Journal of Controlled Release*, 2008, **126**, 50-58

26. Y. Zhou, D.C. Drummond, H. Zou, M.E. Hayes, G.P. Adams, D.B. Kirpotin, et al. Impact of single-chain Fv antibody fragment affinity on nanoparticle targeting of epidermal growth factor receptor-expressing tumor cells. *J Mol Biol*, 2007, **371**, 934-947

27. D.B. Kirpotin, D.C. Drummond, Y. Shao, M.R. Shalaby, K. Hong, U.B. Nielsen, et al. Antibody targeting of long-circulating lipidic nanoparticles does not increase tumor localization but does increase internalization in animal models. *Cancer Research*, 2006, **66**, 6732-40

28. M.S. Goldberg, S.S. Hook, A.Z. Wang, J.W. Bulte, A.K. Patri, F.M. Uckun, et al. Biotargeted nanomedicines for cancer: six tenets before you begin. *Nanomedicine (Lond),* 2013, **8**, 299-308. doi: 10.2217/nnm.13.3.

29. F.M. Uckun, A.L. Burkhardt, L. Jarvis, X. Jun, B. Stealey, I. Dibirdik, et al. Signal transduction through the CD19 receptor during discrete developmental stages of human B-cell ontogeny. *J. Biol. Chem*, 1993, **268***,* 21172-21184

30. F.M. Uckun. Regulation of human B-cell ontogeny (Review). Blood, 1990, ***76,*** 1908-1923

31. B.E. Bejcek, D. Wang, E. Berven, C.A. Pennell, S.C. Peiper, S. Poppema, et al. Development and characterization of three recombinant single chain antibody fragments (scFvs) directed against the CD19 antigen. *Cancer Res*, 1995, **55**, 2346-2351

32. Y. Kong, S. Yoshida, Y. Saito, T. Doi, Y. Nagatoshi, M. Fukata, et al. CD34+CD38+CD19+ as well as CD34+CD38-CD19+ cells are leukemia-initiating cells with self-renewal capacity in human B-precursor ALL. *Leukemia*, 2008, **22**, 1207-13

33. C. Le Viseur, M. Hotfilder, S. Bomken, K. Wilson, S. Rottgers, A. Schrauder, et al. In childhood acute lymphoblastic leukemia, blasts at different stages of immunophenotypic maturation have stem cell properties. *Cancer Cell*, 2008, **14**, 47-58

34. H.J. Varmoor. Malignant stem cells in childhood acute lymphoblastic leukemia. *Cell Cycle*, 2009, **8**, 996-999.

35. F.M. Uckun, S. Qazi, I. Dibirdik, D.E. Myers. Rational design of an immunoconjugate for selective knockdown of leukemia-specific E2A-PBX1 fusion gene expression in human Pre-B leukemia. *Integr Biol (Camb),* 2013, **5**,122-32. doi: 10.1039/c2ib20114c.

36. O.J. D'Cruz, F.M. Uckun. Novel mAb-based therapies for leukemia. In: "*Monoclonal Antibodies in Oncology*", Uckun FM (Ed), Future Medicine 2013, pp 54-77. doi: 10.2217/ebo.13.218. Future Medicine Ltd, London.

37. R. Handgretinger, G. Zugmaier, G. Henze, H. Kreyenberg, P. Lang, A. von Stackelberg. Complete remission after blinatumomab-induced donor T-cell activation in three pediatric patients with post-transplant relapsed acute lymphoblastic leukemia. *Leukemia* , 2011, **25**, 181-4. doi: 10.1038/leu.2010.239.

38. R.J. Brentiens, M.L. Davilla, I Riviera, J. Park, X. Wang, L.G. Cowell, et al. CD19-targeted T cells rapidly induce molecular remissions in adults with chemotherapy-refractory acute lymphoblastic leukemia. *Sci Transl Med*, 2013, **5**, 177ra38. doi: 10.1126/scitranslmed.3005930.

39. J. Zhang, Y. Tang, H. Shen, B. Qian. Targeting and internalization of sterically stabilized liposome modified with ZCH-4-2E8. *J Huazhong Univ Sci Technol*, 2009, **29**, 273-280

Figures and Figure Legends

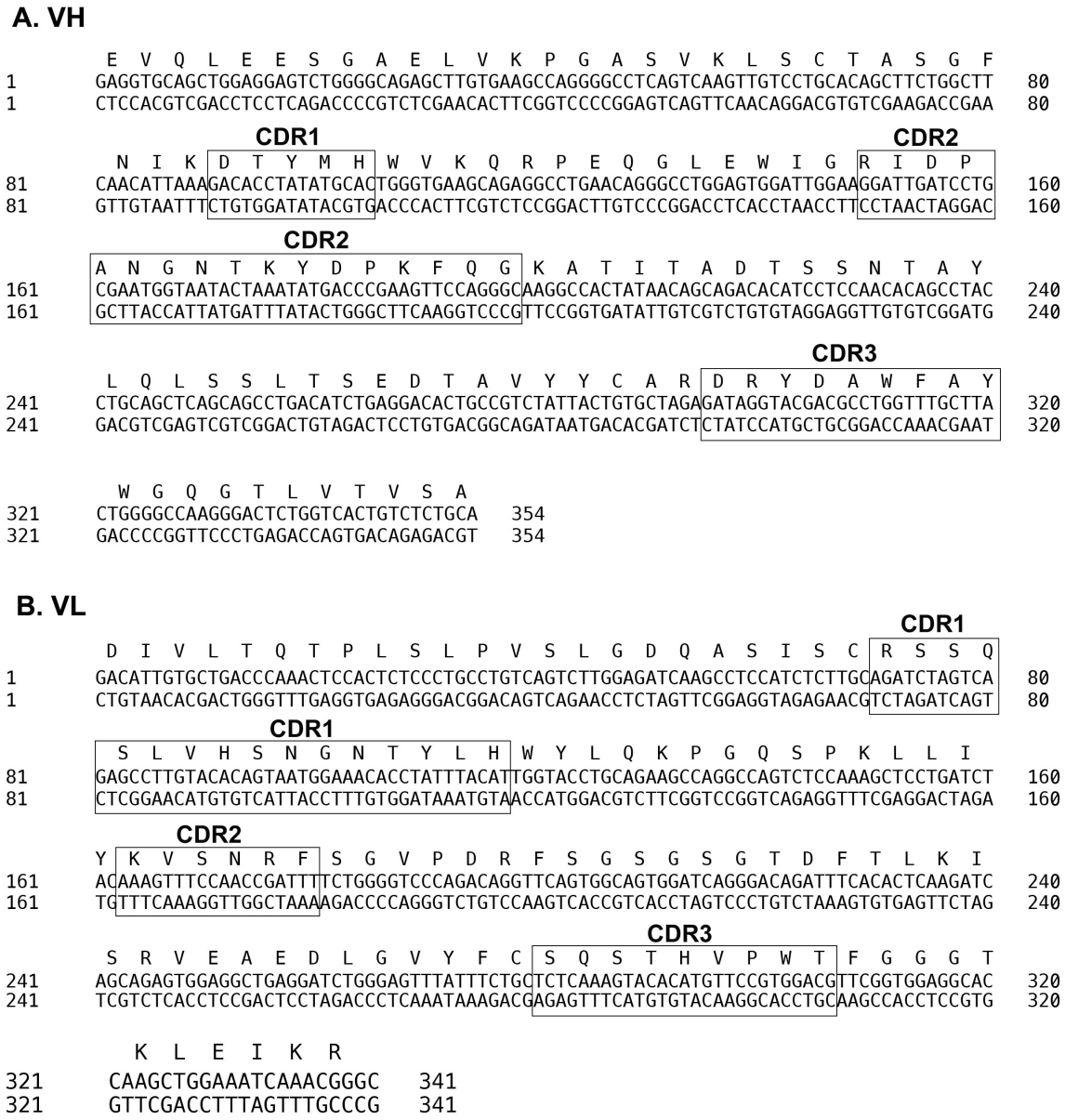

Figure 1. CDR Sequences of the anti-CD19 MoAb. The unique cDNA sequences of the VH and VL CDRs were determined as described in Materials and Methods.

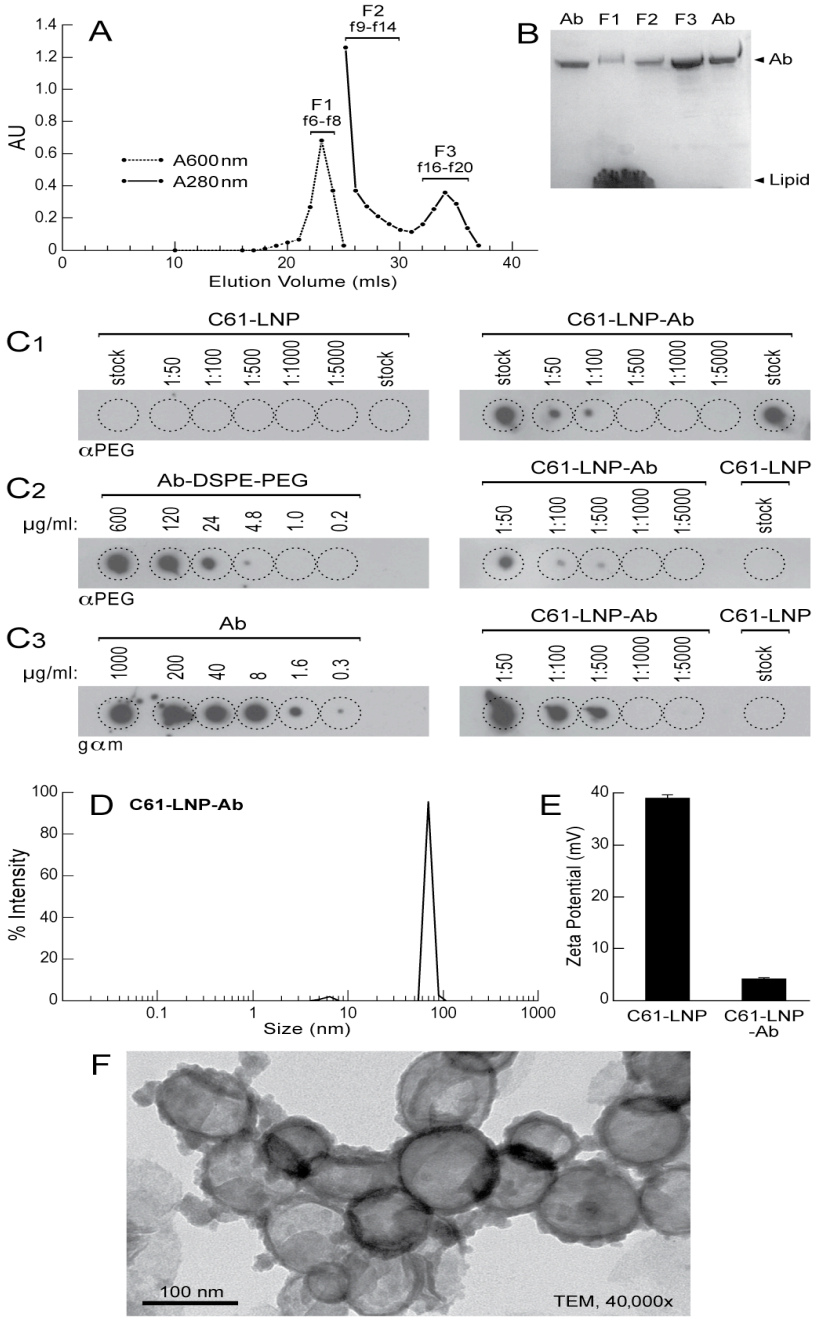

Figure 2. Characteristics of CD19-directed C61-LNP-Ab [A] After decoration of the C61-LNP with DSPE-PEG3400-NHS modified anti-CD19 MoAb, the biotargeted C61-LNP ("C61-LNP-Ab") were separated from uninserted, modified anti-CD19 MoAb using a Sephacryl S-300 HR size-exclusion column. The fractions f6-f8 containing the antibody-modified C61-LNP-Ab were combined as F1 and subjected to further characterization. The peak of antibody typically eluted between 70 and 80 min (f16-f20) after loading and was collected as a combined F3 fraction. Fraction F2 (f9-f14) represents the shoulder of the LNP peak and contains micelles of the modified anti-CD19 MoAb. **[B]** SDS-PAGE was performed under denaturing conditions (SDS) on samples eluting from the S-300 column. 4-20% tris–glycine gradient separating gels were used with no reducing agent.

Staining of the gels with Coomassie Blue showed the presence of both intact antibody and lipid in fraction F1 (from A), which contained the C61-LNP-Ab. There was no lipid apparent in fraction F3, representing the uninserted, anti-CD19 MoAb. The Ab lane contained a sample of the purified anti-CD19 MoAb as a standard for the intact MoAb. **[C]** Dot blot analysis of the PEG and MoAb content of C61-LNP-Ab. The decorating antibody both in unmodified form (Concentration range: 0.3-1000 µg/mL) as well as DSPE-PEG modified form (Concentration range: 0.2-600 µg/mL) used for post-insertion and non-PEGylated C61-LNP was included as controls. The dot blots were performed on PVDF membranes using both a polyclonal rabbit anti-PEG antibody (C1 and C2) as well as a polyclonal goat-anti-mouse IgG antibody (C3). The latter binds to the mouse anti-CD19 MoAb molecules inserted into the liposomal nanoparticles. The immunoreactive dots were visualized by chemiluminescence, as described in Materials and Methods. **[D]** Particle size (radius) measurement of the C61-LNP-Ab using dynamic light scattering indicated a mean diameter of 154.2±1.9 nm (radius: 77.1±0.9 nm) (N=10). [E] Zeta potential of unmodified C61-LNP and C61-LNP-Ab. [F] Transmission electron microscopy (TEM) images of the C61-LNP-Ab.

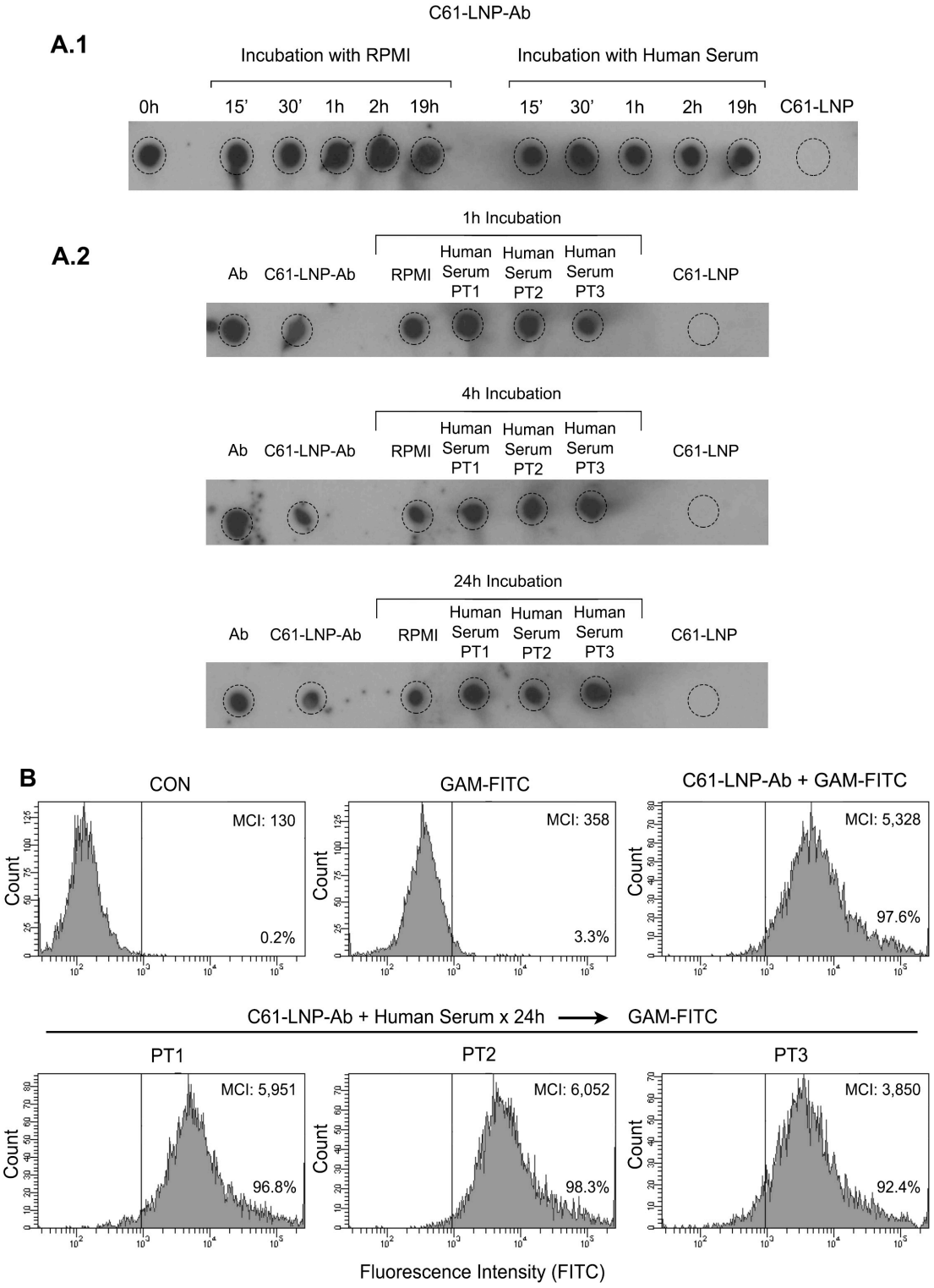

Figure 3. Stability of C61-LNP-Ab in the Presence of Human Serum. C61-LNP-Ab was incubated for indicated time periods ranging from 15 min to 24 h with serum obtained from primary bone marrow aspirate samples of 3 pediatric B-precursor ALL patients (PT1, PT2, PT3) at a 1:1 volume: volume ratio. Subsequently, dot plot analysis of 2 μL aliquots was performed on PVDF

membranes using a polyclonal goat anti-mouse IgG-HRP. Likewise, a flow cytometric immunoreactivity analysis with the B-precursor ALL cell line ALL-1 using the FITC-labeled GAM antibody was performed. Control samples were incubated with serum-free RPMI tissue culture medium instead of human serum. The immunoreactive dots were visualized by chemiluminescence, as described in Materials and Methods. **A.1** depicts the dot blots of the C61-LNP-Ab samples that were incubated with serum from PT1 for 15 min-19 h. **A.2** depicts the dot blots of the C61-LNP-Ab samples that were incubated with serum from PT1, PT-2, or PT3 for 1h, 4h, or 24h. Untreated free Ab served as a positive control whereas C61-LNP served as a negative control. **B.** depicts in the upper row the FACS histograms of the B-precursor ALL cell line ALL-1 stained for 1 h on ice with GAM-FITC alone or C61-LNP-Ab (200 µg/mL based on C61 content) followed by GAM-FITC. Control ALL-1 cells (CON) were left unstained. Depicted in the bottom row are the FACS histograms of ALL-1 cells stained with C61-LNP-Ab that was preincubated for 24h with human serum from PT1, PT2, or PT3. MCI: median channel of immunofluorescence. The percentage of cells displaying above background fluorescence is indicated for each sample.

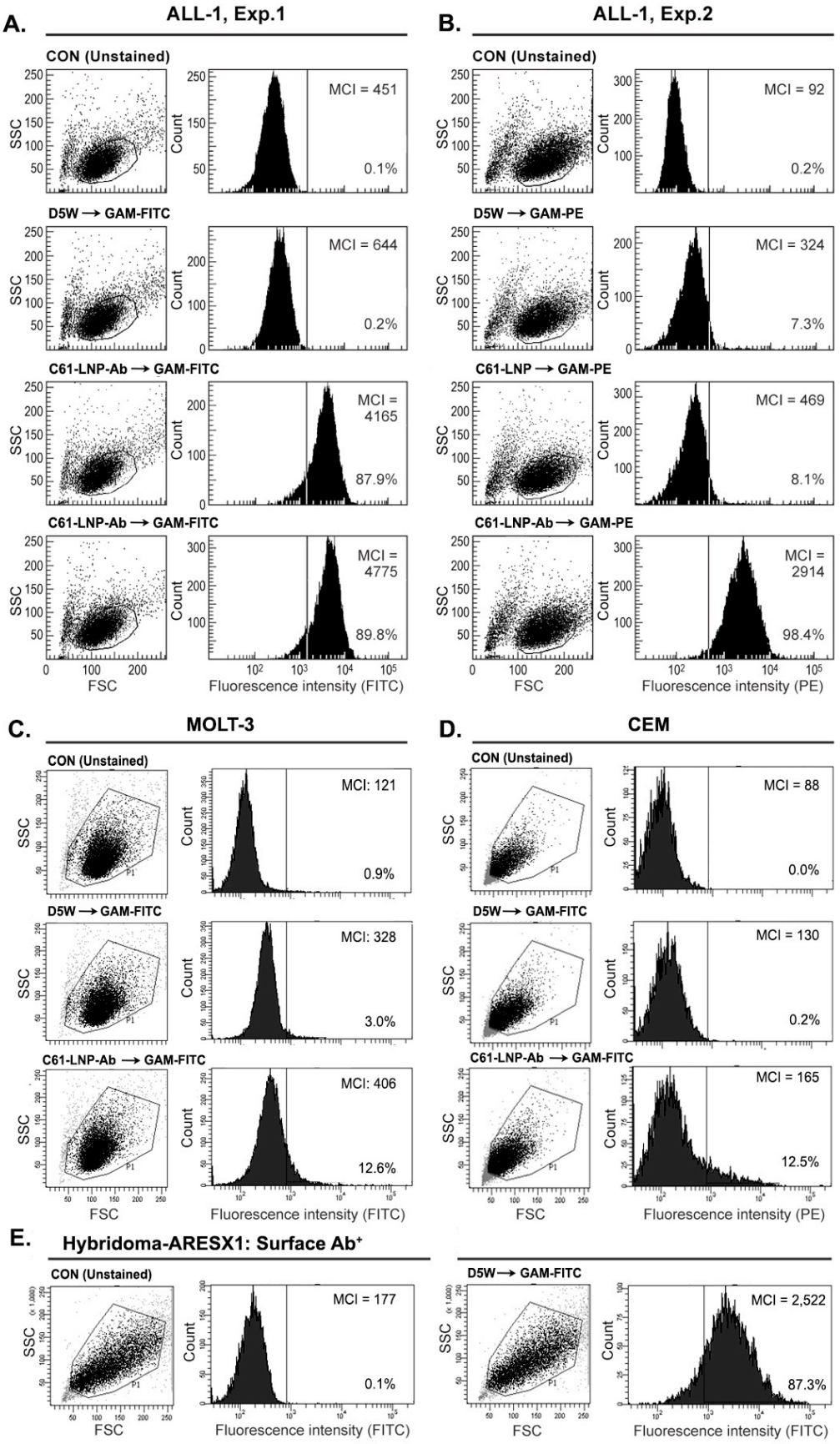

Figure 4. Immunoreactivity of Antibody-Decorated C61-LNP-Ab with B-Precursor ALL

Cells. The immunoreactivity of the C61-LNP-Ab with the CD19-receptor positive B-precursor ALL cell line ALL1 (BCR-ABL$^+$, Pre-pre-B) was examined by standard indirect immunofluorescence and flow cytometry using FITC- (Experiment 1, Panel A) or PE-labeled goat anti-mouse (GAM) antibodies (Experiment 2, Panel B) to detect the cell-bound murine anti-CD19 MoAb moiety of the C61-LNP-Ab. Depicted are two-parameter (FSC/SSC) light scatter dot plots and single-color fluorescence histograms of ALL-1 cells stained with C61-LNP-Ab. Controls included unstained cells, cells stained with GAM alone, as well as cells stained with C61-LNP (as a non-immunoreactive LNP control). The concentration of the C61-LNP-Ab (based on C61 content) was 200 µg/mL in 3rd row in A and 400 µg/mL in 4th row in Panel A & B. The lack of a marked difference between the percent binding at the two concentrations indicates that a near complete target CD19-receptor saturation is achieved at the 200 µg/mL concentration. The concentration of C61-LNP in B was 200 µg/mL based on C61 content. The interaction of C61-LNP-Ab (400 µg/mL based on C61 content) with CD19-receptor negative human cells was also examined using two different T-lineage ALL cell lines. C61-LNP-Ab did not bind to MOLT-3 (Panel C) or CEM (Panel D) cell lines as it did to ALL-1 cells. The small percentages of MOLT3 and CEM cells (<15%) showing above background fluorescence likely reflect the ability of liposomes to interact with cellular membranes. The poor binding of C61-LNP-Ab to the CD19-receptor negative T-lineage ALL cell lines was not a false negative result caused by a technical problem related to the secondary antibody GAM-FITC, because the latter antibody exhibited strong binding to the murine hybridoma cell line ARESX1 expressing the antibody moiety of C61-LNP-Ab on its surface (panel E). MCI: Median channel of immunofluorescence. Depicted in each FACS histogram are the MCI values and the percentages of cells with above background fluorescence.

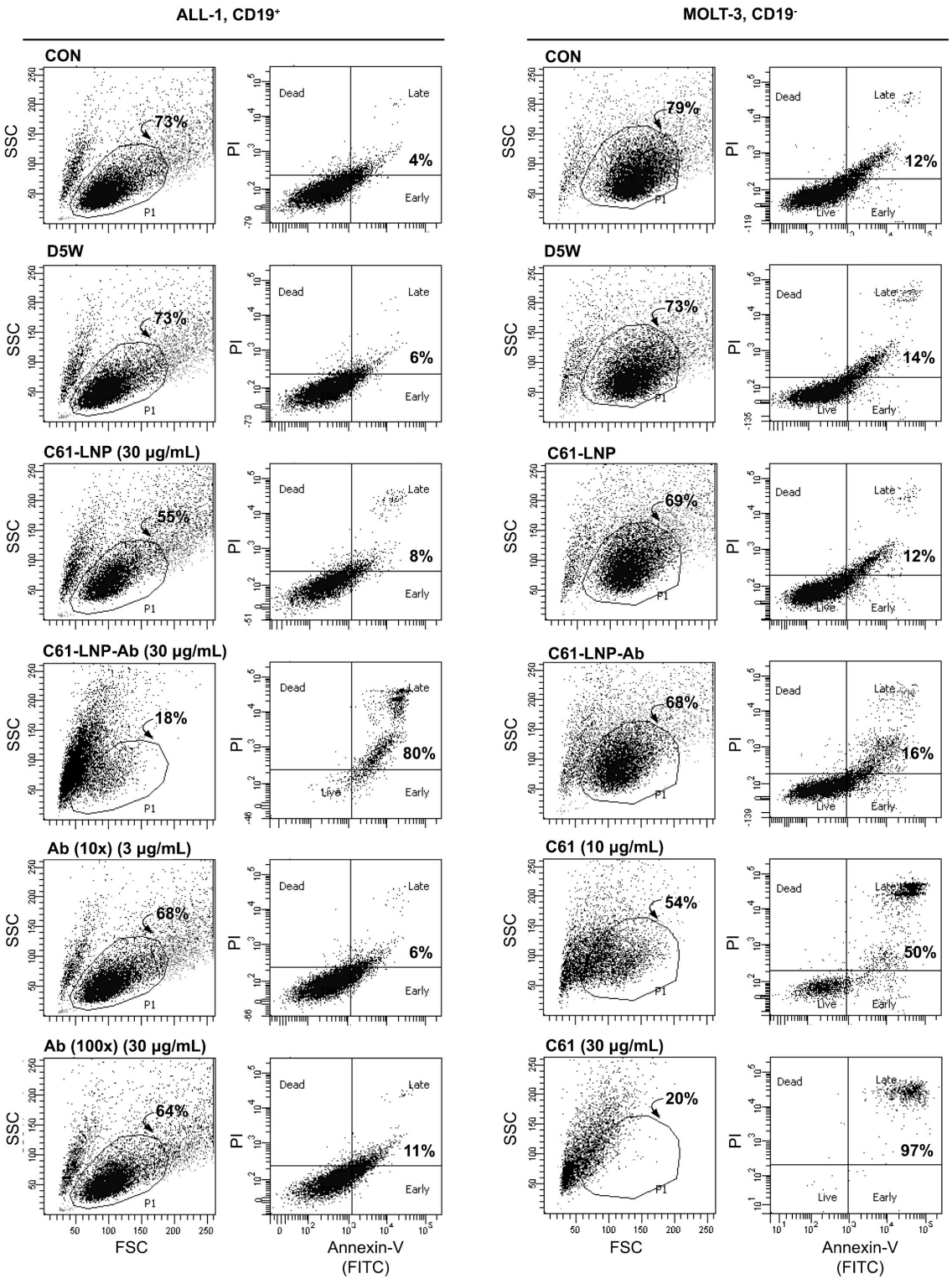

Figure 5. C61-LNP-Ab induces apoptosis in CD19+ ALL cells but not in CD19- ALL cells. Two-color fluorescence density plots of CD19+ B-precursor ALL cell line ALL-1 and CD19- T-lineage ALL cell line MOLT-3 that were treated for 48 h at 37°C with unmodified (C61-LNP, 30 µg/mL based

on C61 content) or antibody-decorated C61-LNP (C61-LNP-Ab, 30 μg/mL based on C61 content; estimated Ab content = 0.3 μg/mL). Controls included D5W-treated cells as well as untreated control cells (CON) and cells treated with the anti-CD19 MoAb used in the preparation of C61-LNP-Ab. The Ab was used at 3 μg/mL and 30 μg/mL concentrations representing 10-fold (i.e. 10x) and 100-fold (i.e. 100x) higher concentrations than the antibody content of the C61-LNP-Ab samples tested (30 μg/mL concentration based on the C61 content). MOLT-3 cells were also treated with unformulated C61 (dissolved in DMSO) at a 10 μg/mL or 30 μg/mL concentration. Cells were analyzed for apoptosis using the standard quantitative flow cytometric apoptosis assay using the Annexin V-FITC Apoptosis Detection Kit from Sigma as discussed in the Methods section. The labeled cells were analyzed on a LSR II flow cytometer. D5W = water with 5% dextrose

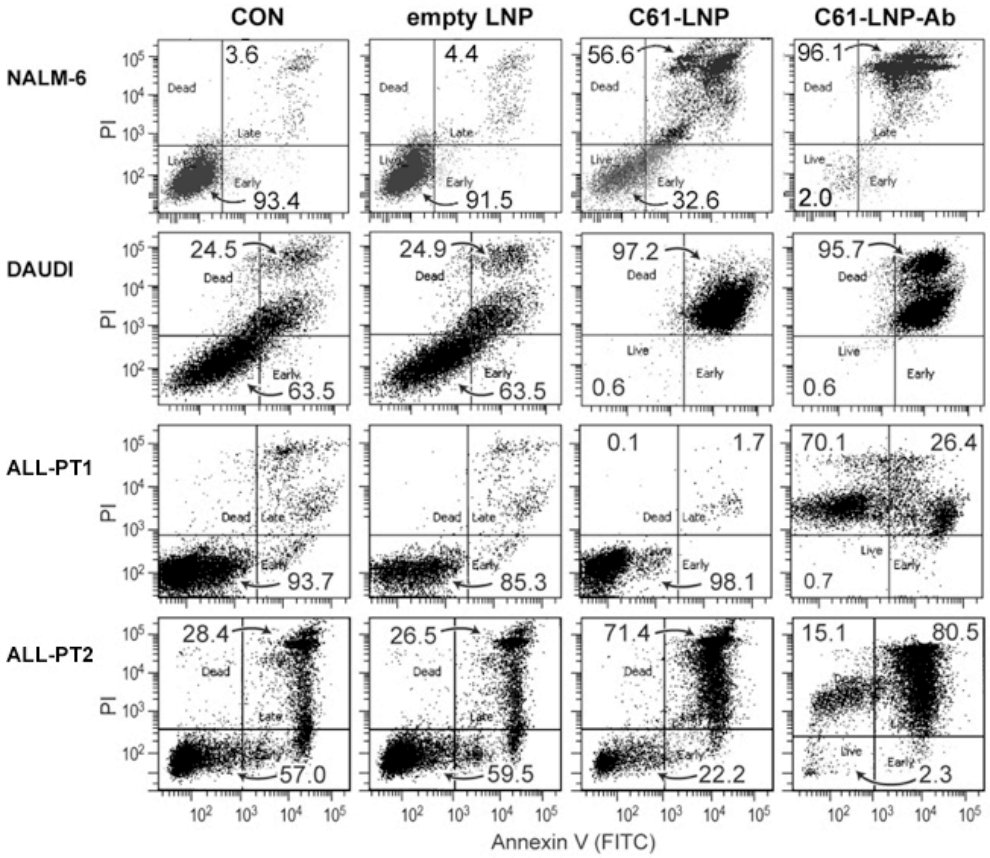

Figure 6. In Vitro Anti-leukemic Potency of Unmodified and Antibody-Decorated C61-LNP Against Leukemia Cell Lines and Primary B-precursor ALL Cells. Representative two-color fluorescence density plots of leukemia cell lines (NALM-6 and DAUDI) and primary leukemia cells from 2 pediatric B-precursor ALL patients (ALL-PT1 and ALL-PT2). The PI fluorescence intensity is depicted along the Y-axis and the Annexin V (FITC) fluorescence is depicted along the X-axis. Cells were treated for 48 h at 37^{o}C with unmodified (C61-LNP, 30 μg/mL) or antibody-decorated C61-LNP (C61-LNP-Ab, 30 μg/mL). Controls included sham-treated cells (CON) and cells treated with empty LNP (C61-free empty LNP with the same lipid content as C61-LNP used at 30 μg/mL C61-based concentration). Cells were analyzed for apoptosis using the standard quantitative flow cytometric apoptosis assay using the Annexin V-FITC Apoptosis Detection Kit from Sigma as discussed in the Methods section. The labeled cells were analyzed on a LSR II flow cytometer. C61-LNP-Ab caused apoptosis in the vast majority of treated B-precursor ALL cells. The anti-leukemic potency of C61-LNP is evidenced by the significantly lower percentages of Annexin V-FITC^{-}PI^{-} live cells located in the left lower quadrant of the corresponding two-color fluorescence density plots as well as a

substantially higher percentage of Annexin V-FITC^{+}PI^{+} apoptotic cells located in the right upper quadrant. The cumulative results are depicted in Figure 7.

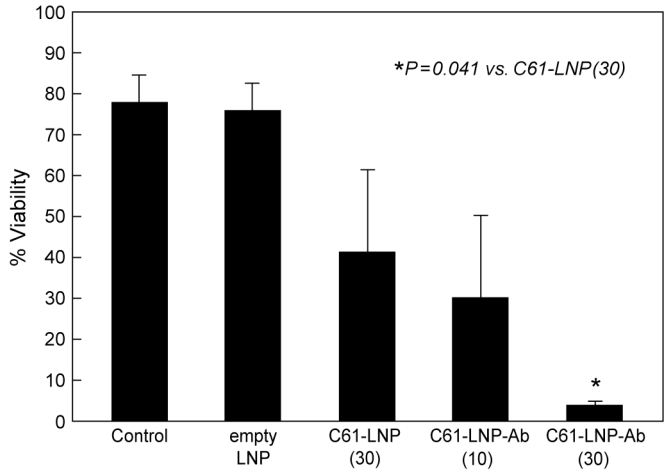

Figure 7. In Vitro Anti-leukemic Potency of Unmodified C61-LNP and C61-LNP-Ab Against B-precursor ALL Cells. Depicted are bar graphs showing the percent viability of pediatric (age at the time of diagnosis ≤21 years) B-precursor ALL cells (N=4; primary leukemia cells from 3 pediatric patients with B-precursor ALL, and pediatric B-precursor ALL cell line NALM-6 derived from a 19-year old patient) after sham treatment (N=8, no liposomes, drugs, or antibody), treatment with 30 µg/mL C61-LNP (N=4), empty LNP (N=3), and 10 µg/mL (N=3) or 30 µg/mL (N=4) C61-LNP-Ab. The viability was measured using a flow cytometric quantitative apoptosis assay. The percent viability values represent the percentage of Annexin V-FITC$^-$PI$^-$ live cells located in the left lower quadrant of the corresponding two-color fluorescence density plots. Control: Sham-treated samples; empty LNP: C61-free empty LNP with the same lipid content as C61-LNP used at 30 µg/mL C61-based concentration. The numbers in parentheses indicate the C61 payload amount in µg/mL. The mean percentages of viable, non-apoptotic cells after various treatments were 78.1±6.5 % (N=8) for sham-treated (no liposomes, drugs, or antibody) control samples, 76.0±6.6% (N=3) for empty LNP not loaded with C61, 41.4±19.9% (N=4) for unmodified C61-LNP (30 µg/mL C61; P [vs. control] = 0.023), 30.2±20.0% (N=3) for C61-LNP-Ab at 10 µg/mL C61 (P[vs. control] = 0.009) and 3.9±1.1% (N=4) for C61-LNP-Ab at 30 µg/mL C61 (P [vs. control] = 0.0001; P[vs. 30 µg/mL unmodified C61-LNP] = 0.041).

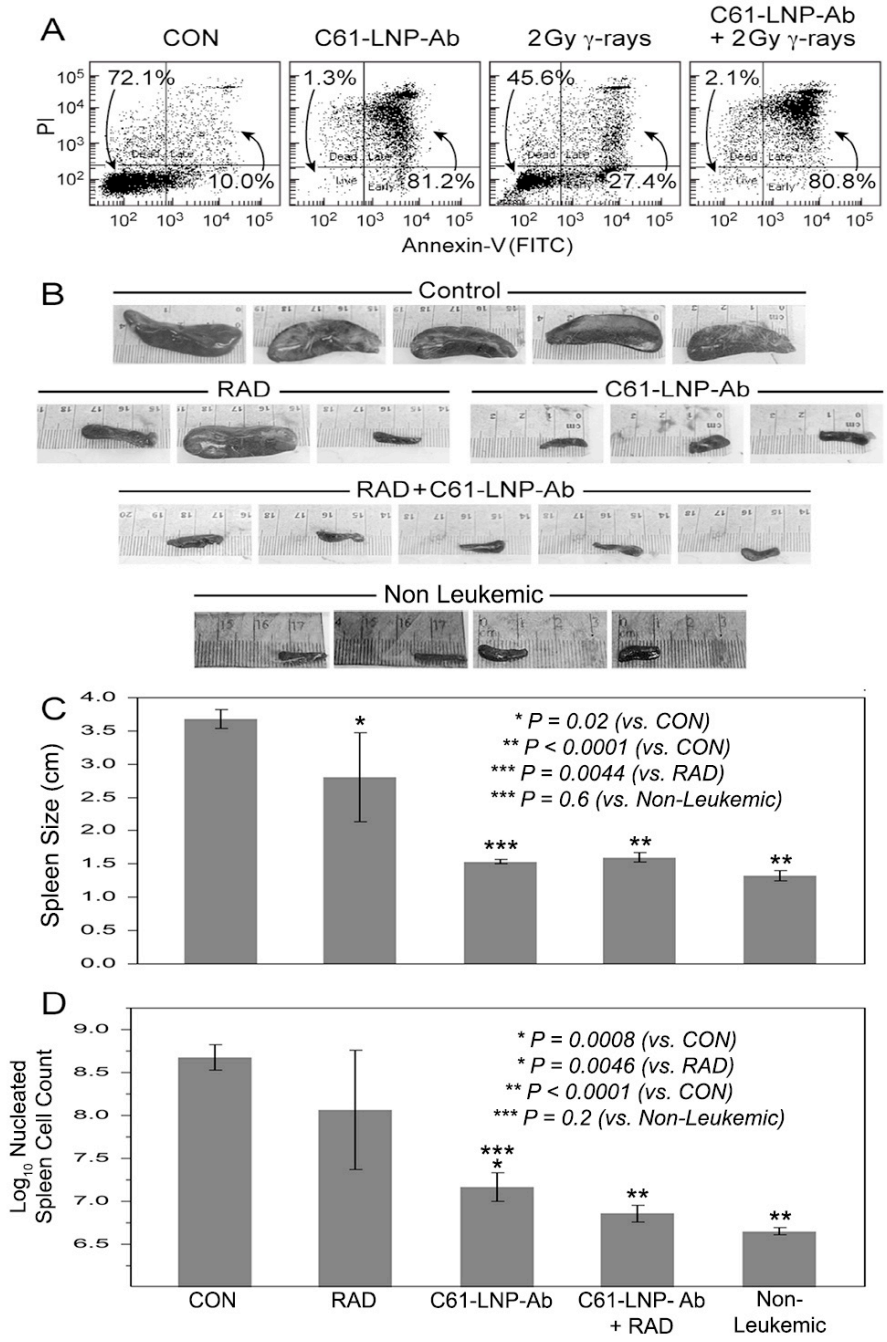

Figure 8. Anti-leukemic Effects of C61-LNP-Ab + Radiation Against Leukemia-Initiating In Vivo Clonogenic B-precursor ALL Xenograft Cells. [A] Two-color fluorescence dot plots of ALL xenograft cells that were treated for 48 h at 37°C with C61-LNP-Ab, 2 Gy γ-rays, or C61-LNP-Ab+2Gy γ-rays. Controls (CON) included D5W-treated cells. Cells were analyzed for apoptosis using the standard quantitative flow

cytometric apoptosis assay using the Annexin V-FITC Apoptosis Detection Kit from Sigma. The labeled cells were analyzed on a LSR II flow cytometer. C61-LNP-Ab alone or in combination with radiation caused apoptosis in the vast majority of treated xenograft cells. The anti-leukemic potency of C61-LNP-Ab is evidenced by the significantly lower percentages of Annexin V-FITC^{-}PI^{-} live cells located in the left lower quadrant of the corresponding two-color fluorescence intensity dot plots as well as a substantially higher percentage of Annexin V-FITC^{+}PI^{+} apoptotic cells located in the right upper quadrant than in the control sample. **[B]** Depicted are the spleen images of NOD/SCID mice challenged with xenograft cells that have been exposed to various treatments. The spleen images were obtained using an iPhone 4S equipped with an 8-megapixel iSight camera (Apple, Cupertino, CA). NOD/SCID mice challenged with untreated xenograft ALL cells rapidly developed overt leukemia with massive splenomegaly. By contrast, the spleens of mice challenged with C61-LNP-Ab or C61-LNP-Ab + radiation treated xenograft ALL cells had a normal size. See text for detailed discussion. **[C]** Depicted are the bar graphs of the mean spleen sizes of NOD/SID mice shown in B. **[D]** Depicted are the bar graphs of the log-transformed spleen nucleated cell counts of NOD/SCID mice shown in B. The average spleen nucleated cell count (in millions) as a measure of the leukemic burden was 598±195 (“very high”; $\log_{10}$ = 2.7±0.1) for the control group, 542±450 (“very high”; $\log_{10}$ = 2.1±0.7; P-value = 0.11) for the radiation alone group, 17±6 (“normal”; $\log_{10}$ = 1.2±0.2; P-value = 0.0008; P=0.19 vs. Non-Leukemic) for the C61-LNP-Ab alone group, 8.1±2.2 (“normal”; $\log_{10}$ = 0.86±0.10; P-value < 0.0001 vs. Control; P=0.54 vs. Non-Leukemic) for the C61-LNP-Ab + radiation group, and 4.6±0.4 (“normal”; $\log_{10}$ = 0.65±0.04; P-value < 0.0001 vs Control) for the non-leukemic mice. D5W = water with 5% dextrose

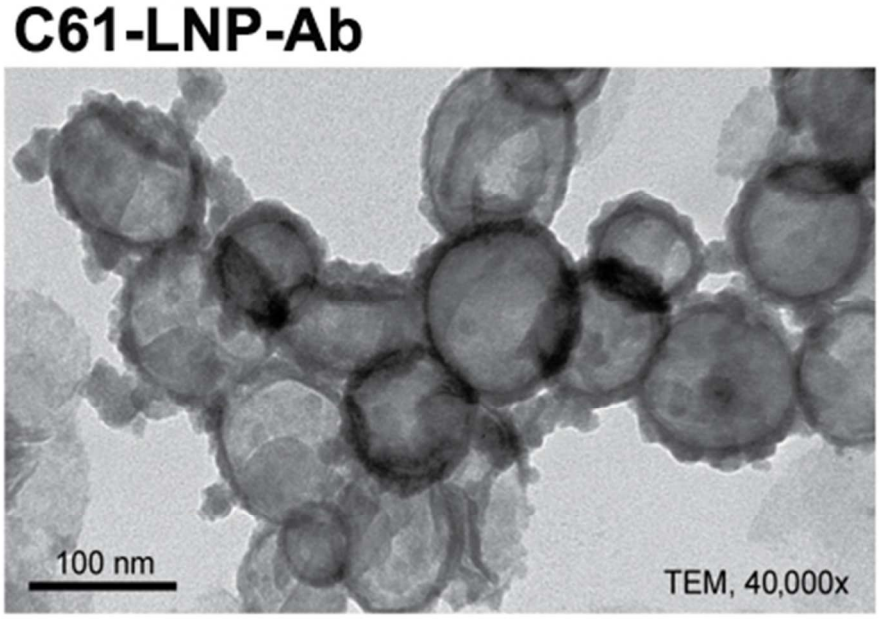

164x113mm (72 x 72 DPI)